

OPEN ACCESS

EDITED BY Luis Diambra, National University of La Plata, Argentina

REVIEWED BY

Alan Givré, National Scientific and Technical Research Council (CONICET), Argentina Juan Ignacio Marrone, National Scientific and Technical Research Council (CONICET), Argentina

*CORRESPONDENCE Irene Zorzan, ☑ zorzan.irene@gmail.com Massimo Bellato, ☑ massimo.bellato@unipd.it

[†]These authors have contributed equally to this work and share last authorship

RECEIVED 26 August 2025 ACCEPTED 19 September 2025 PUBLISHED 21 October 2025

CITATION

Zorzan I, Cimolato C, Schenato L and Bellato M (2025) Structural properties and asymptotic behavior of bacterial two-component systems. *Front. Syst. Biol.* 5:1693064. doi: 10.3389/fsysb.2025.1693064

COPYRIGHT

© 2025 Zorzan, Cimolato, Schenato and Bellato. This is an open-access article distributed under the terms of the Creative Commons Attribution License (CC BY). The use, distribution or reproduction in other forums is permitted, provided the original author(s) and the copyright owner(s) are credited and that the original publication in this journal is cited, in accordance with accepted academic practice. No use, distribution or reproduction is permitted which does not comply with these terms.

Structural properties and asymptotic behavior of bacterial two-component systems

Irene Zorzan^{1*}, Chiara Cimolato¹, Luca Schenato^{1†} and Massimo Bellato^{1,2*†}

¹Department of Information Engineering, Università degli Studi di Padova, Padova, Italy, ²Department of Molecular Medicine, Università degli Studi di Padova, Padova, Italy

Bacteria rely on two-component signaling systems (TCSs) to detect environmental cues and orchestrate adaptive responses. Despite their apparent simplicity, TCSs exhibit a rich spectrum of dynamic behaviors arising from network architectures, such as bifunctional enzymes, multi-step phosphorelays, transcriptional feedback loops, and auxiliary interactions. This study develops a generalized mathematical model of a TCS that integrates these various elements. Using systems-level analysis, we elucidate how network architecture and biochemical parameters shape key properties such as stability, monotonicity, and signal amplification. Analytical conditions are derived for when the steady-state levels of phosphorylated proteins exhibit robustness to variations in protein abundance. The model characterizes how equilibrium phosphorylation levels depend on the absolute and relative abundances of the two components. Specific scenarios are explored, including the MprAB system from Mycobacterium tuberculosis and the EnvZ/ OmpR system from textit Escherichia coli, to describe the potential role of reverse phosphotransfer reactions. By combining mechanistic modeling with systemlevel techniques, such as nullcline analysis, this study offers a unified perspective on the design principles underlying the versatility of bacterial signal transduction. The generalized modeling framework lays a theoretical foundation for interpreting experimental dynamics and rationally engineering synthetic TCS circuits with prescribed response dynamics.

KEYWORDS

two-component systems, MprAB *Mycobacterium*, EnvZ, OmpR, synthetic biology, sensor histidine kinase, response regulator, odes

1 Introduction

Bacteria rely on two-component systems (TCSs) as their primary signaling modules to detect environmental cues and orchestrate adaptive responses. A canonical TCS consists of a membrane-bound sensor histidine kinase (SHK) and a cytoplasmic response regulator (RR). Upon stimulation, the SHK autophosphorylates on a conserved histidine and transfers the phosphoryl group to an aspartate on the RR, generating the active form (RR-P) that typically regulates gene expression. This minimal architecture is remarkably versatile, underpinning processes such as chemotaxis, nutrient sensing, antibiotic resistance, and virulence regulation (Tierney and Rather, 2019; Tiwari et al., 2017; Kirby, 2009; Ramos et al., 2022; Alvarez and Georgellis, 2023).

Despite their apparent simplicity, TCSs display a rich spectrum of topologies and dynamic behaviors (Zschiedrich et al., 2016; Groisman, 2016; Stock et al., 2000). In some

TABLE 1 Comparison of previous findings on bacterial TCSs with results from this study's model.

References	Findings from previous studies	Model results of this study
Batchelor and Goulian (2003)	Robustness of RR-P steady-state levels when SHK is limiting; EnvZ/OmpR experiments confirmed robustness to fluctuations in protein abundance.	Reproduces robustness when exogenous phosphorylation is absent. Predicts loss of robustness (steady state depends on SHK:RR ratio) if exogenous phosphorylation flux is present.
Shinar et al. (2007)	Formalized conditions for input-output robustness; robustness breaks down when multiple phosphorylation/dephosphorylation pathways exist.	General model confirms robustness only under restricted architectures. Multiple independent routes compromise robustness.
(Dutta and Inouye, 1996); (Zhu et al., 2000)	Proposed and observed reverse phosphotransfer (RR-P \rightarrow SHK) in EnvZ/OmpR; debated as mechanism for phosphatase activity.	Extends framework to include reverse phosphotransfer. Predicts that it does not affect RR-P steady state (compensated by forward transfer), but increases phosphorylated SHK levels.

systems, exemplified by CheA in bacterial chemotaxis, SHK functions exclusively as a kinase, phosphorylating the RR. However, in many TCSs, SHK is bifunctional, participating in both phosphorylation and dephosphorylation of its cognate RR. In such cases, the input signal can modulate either one or both of these enzymatic activities, effectively tuning the rates of kinase and/or phosphatase reactions. TCSs may implement single-step phosphotransfers or multi-step phosphorelays, adding regulatory complexity and potentially delaying signal propagation.

At the transcriptional level, many TCSs feature autoregulation: the phosphorylated RR activates transcription of both its own gene and the gene encoding its partner SHK, thereby forming a positive feedback loop (Goulian, 2010). This feedback can alter steady-state behavior, activation, and inactivation kinetics and generate transient overshoot or "memory" effects, whereby the system responds faster repeated stimuli. Although less common, autoregulation—or even mixed positive and feedback—has been observed in specific systems, providing an additional layer of response modulation. Auxiliary proteins can further diversify TCS behaviors, either by directly interacting with SHKs or RRs or by mediating cross-talk between otherwise independent TCS pathways (Rao et al., 2021; Groisman, 2016).

Mathematical modeling has been pivotal in elucidating the emergent properties of TCSs (summarized in Table 1). Batchelor and Goulian (2003) demonstrated that the steady-state level of RR-P can be robust to protein abundance fluctuations when SHK is limiting, a property supported by experimental data. Shinar et al. (2007) formalized the conditions for input-output robustness, showing that robustness is compromised when multiple independent phosphorylation or dephosphorylation routes exist. Igoshin et al. (2008) identified conditions for bistability, particularly when unphosphorylated SHK and RR form "dead-end" complexes or when alternative phosphatases modulate RR-P turnover. Ray and Igoshin (2010), Mitrophanov et al. (2010), and Zorzan et al. (2021) explored the role of transcriptional feedback, showing that autoregulation can alter response speed, overshoot amplitude, and even affect the effective sign of feedback, enabling TCSs to switch between positive and negative regulatory modes depending on signal strength. These studies collectively highlight how bifunctionality, phosphorelays, and feedback loops produce rich dynamic behaviors—including robustness, bistability, and adaptive memory—that are now central themes in systems-level analyses of TCSs.

In this study, we develop a systems-level model of a generalized TCS model focusing on the MprAB system from *Mycobacterium tuberculosis* that integrates canonical phosphorylation cycles, bifunctional enzymatic activity, transcriptional feedback, and potential auxiliary interactions. Our modeling framework seeks to (i) dissect how network architecture and parameter regimes shape dynamic properties and provide robustness, to be adopted as a building block to implement overshoots, oscillations, and bistability, and (ii) provide a predictive foundation for interpreting experimental dynamics and guiding synthetic circuit design in bacterial signal transduction.

By combining mechanistic modeling with systems-level analysis, this study elucidates how bifunctionality, phosphorelays, and feedback loops shape the dynamic behavior of TCSs, providing insights into bacterial adaptation and a framework for the rational engineering of synthetic signaling circuits (Mukherji and van Oudenaarden, 2009; Pasotti et al., 2017; Müller et al., 2025).

2 Two-component system: mathematical model

The model we consider is a general version of the model proposed in Tiwari et al. (2010) to describe the functioning of the two-component system *MprA/MprB* in *M. tuberculosis* in its active state.

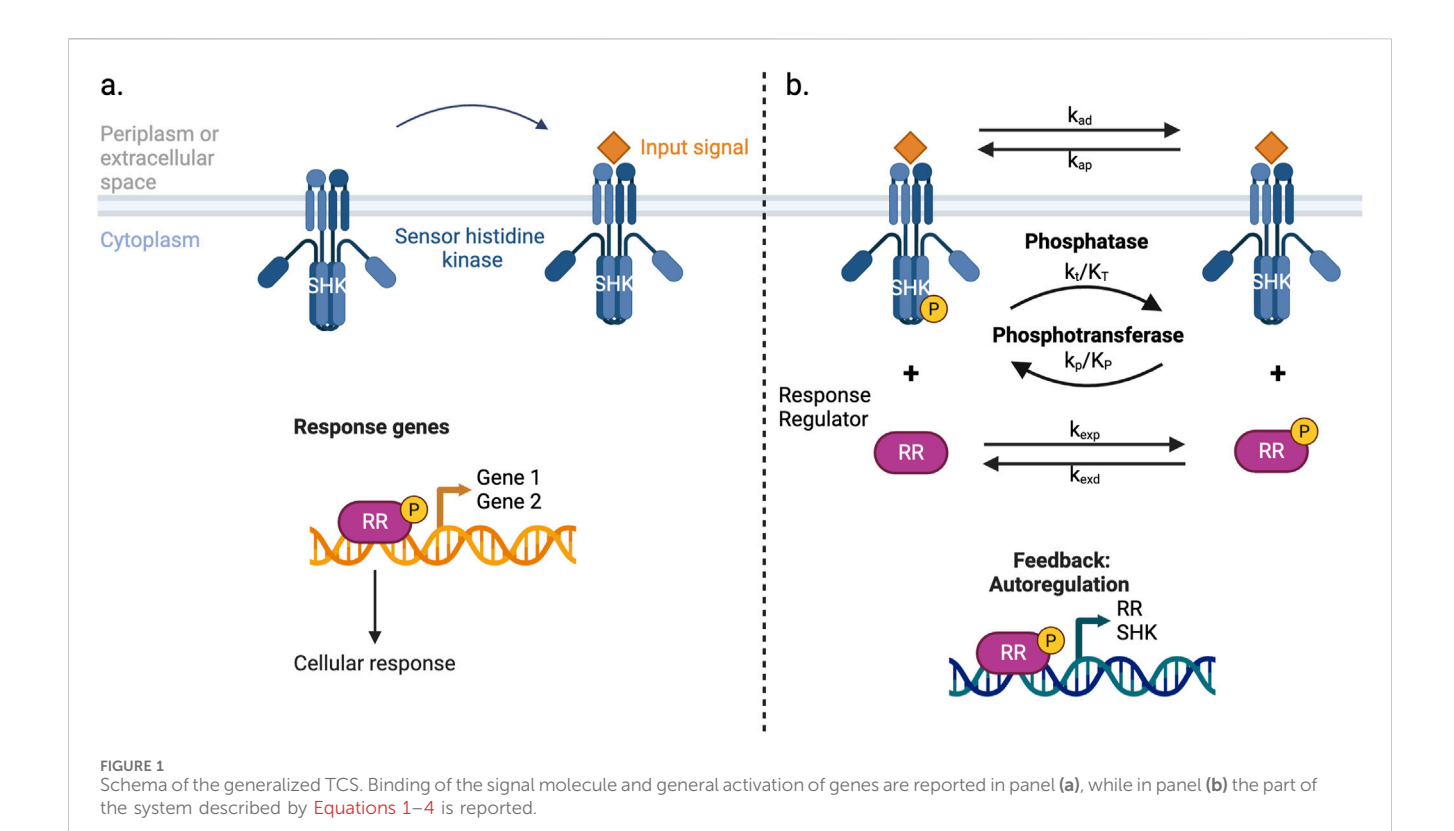
For the sake of generality, we refer to "response regulator" (RR) and "sensor histidine kinase" (SHK) rather than to MprA and MprB, respectively. Denoting by r (r^*) and s (s^*), the concentration of RR (phosphorylated RR) and SHK (phosphorylated SHK), respectively, the dynamic evolution of the two-component system is described by the following set of ODEs (see Supplemental Information of Tiwari et al. (2010), Equations (S39)–(S42)):

$$\dot{r} = \frac{k_p}{K_p} r^* s - \frac{k_t}{K_T} r s^* + k_{exd} r^* - k_{exp} r + \nu_r - k_{pdeg} r \tag{1}$$

$$\dot{r}^* = -\frac{k_p}{K_D} r^* s + \frac{k_t}{K_D} r s^* - k_{exd} r^* + k_{exp} r - k_{pdeg} r^*$$
 (2)

$$\dot{s} = k_{ad}s^* - k_{ap}s + \frac{k_t}{K_T}rs^* + \nu_s - k_{pdeg}s \tag{3}$$

$$\dot{s}^* = -k_{ad}s^* + k_{ap}s - \frac{k_t}{K_T}rs^* - k_{pdeg}s^*$$
 (4)



-where

- v_r and v_s are the production rate constants of *RR* and *SHK*, respectively;¹
- k_p is the rate constant for the *SHK*-dependent dephosphorylation of RR^* ;
- K_P is the Michaelis-Menten constant for RR* dephosphorylation by SHK;
- k_t is the rate constant for the SHK^* -dependent phosphorylation of RR;
- K_T is the Michaelis-Menten constant for RR-SHK* phosphotransfer;
- k_{exp} and k_{exd} are the exogenous phosphorylation and dephosphorylation rate constants, respectively;
- k_{ap} and k_{ad} are the autophopshorylation and autodephosphorylation rate constants, respectively;
- k_{pdeg} is the protein degradation rate (assumed equal for RR and SHK).

One additional assumption worth highlighting is that the system is always considered to be in the active state. This is biologically reasonable as external stimuli often saturate the sensing capacity of the TCS. As a result, the transition of the

sensor *s* from the inactive to the active state upon binding external stimuli can be neglected in the model, as well as the availability of ATP inside the cell to provide phosphate groups for the phosphorylation steps.

The overall system can be represented as in Figure 1.

We define the total amount of RR and SHK as $R_T = r + r^*$ and $S_T = s + s^*$, respectively, and rewrite the previous model presented in Equations 1–4 in the form shown in Equations 5–8:

$$\dot{R}_T = k_{pdeg} \left(u_r - R_T \right) \tag{5}$$

$$\begin{split} \dot{r}^* &= -\frac{k_p}{K_P} r^* (S_T - s^*) + \frac{k_t}{K_T} \left(R_T - r^* \right) s^* - k_{exd} r^* + k_{exp} \left(R_T - r^* \right) \\ &- k_{bdea} r^* \end{split}$$

(6)

$$\dot{S}_T = k_{pdeg} (u_s - S_T) \tag{7}$$

$$\dot{s}^* = -k_{ad}s^* + k_{ap}(S_T - s^*) - \frac{k_t}{K_T}(R_T - r^*)s^* - k_{pdeg}s^*$$
 (8)

—where $u_r := v_r/k_{pdeg}$ ($u_s := v_s/k_{pdeg}$) is the net production rate of RR (SHK). Due to the separation of timescales between protein accumulation and phosphorylation/dephosphorylation events, we can assume that total concentrations of RR and SHK are preserved—namely, that R_T and S_T are constant. Under this assumption, we can normalize all state variables and consider the phosphorylated portion of RR and SHK

$$\mathbb{F}^* := \frac{r^*}{R_T}$$
 and $\mathbb{S}^* := \frac{s^*}{S_T}$,

the dynamics of which are described by

¹ Actually, in (Tiwari et al., 2010) production of RR and SHK is described by the summation of two activating Hill functions. As explained later, since we are focusing on the functioning of the Two-Component System, the separation of time scales allows us to assume constant production rates.

$$\begin{split} \dot{\mathbb{r}}^* &= - \Big(k_{exd} + k_{exp} + k_{pdeg} \Big) \mathbb{r}^* - \frac{k_p}{K_p} S_T \mathbb{r}^* (1 - \mathbb{s}^*) - \frac{k_t}{K_T} S_T \mathbb{r}^* \mathbb{s}^* \\ &\quad + \frac{k_t}{K_T} S_T \mathbb{s}^* + k_{exp} \\ \dot{\mathbb{s}}^* &= - \Big(k_{ad} + k_{ap} + k_{pdeg} \Big) \mathbb{s}^* - \frac{k_t}{K_T} R_T \mathbb{s}^* (1 - \mathbb{r}^*) + k_{ap} \end{split}$$

Since we aim to provide a model describing the functioning of *general* two-component systems (TCSs) and unveiling its structural and asymptotic properties, from now on we will consider the following general formulation:

$$\dot{\mathbb{F}}^{*} = -(\alpha_{1} + \alpha_{2})\mathbb{F}^{*} - \alpha_{3}S_{T}\mathbb{F}^{*}(1 - \mathbb{S}^{*}) - \alpha_{4}S_{T}\mathbb{F}^{*}\mathbb{S}^{*} + \alpha_{4}S_{T}\mathbb{S}^{*}$$

$$+ \alpha_{2} =: f_{1}(\mathbb{F}^{*}, \mathbb{S}^{*})$$

$$\dot{\mathbb{S}}^{*} = -(\beta_{1} + \beta_{2})\mathbb{S}^{*} - \beta_{3}R_{T}\mathbb{S}^{*}(1 - \mathbb{F}^{*}) - \beta_{4}R_{T}\mathbb{F}^{*}\mathbb{S}^{*} + \beta_{4}R_{T}\mathbb{F}^{*}$$

$$+ \beta_{2} =: f_{2}(\mathbb{F}^{*}, \mathbb{S}^{*})$$

$$(10)$$

Differential Equations 9, 10 describe the dynamics of the phosphorylated portions of RR and SHK—that is, ratio phosphorylated-RR (phosphorylated-SHK) over total RR (SHK)—under the assumption that total concentrations R_T and S_T are constant. Notice that in Equation 10, the terms $-\beta_4 R_T \mathbb{F}^* \mathbb{S}^*$ and $\beta_4 R_T \mathbb{F}^*$ have been included for reasons of symmetry. Of course, this general formulation can be tailored to the specific two-component system under investigation. For instance, we immediately verify that, upon defining

$$\alpha_1 = k_{exd} + k_{pdeg}, \ \alpha_2 = k_{exp}, \ \alpha_3 = \frac{k_p}{K_P}, \ \alpha_4 = \frac{k_t}{K_T}, \\
\beta_1 = k_{ad} + k_{pdeg}, \ \beta_2 = k_{ap}, \ \beta_3 = \frac{k_t}{K_T}, \ \beta_4 = 0,$$

Equations 9, 10 reduce to the *MprA-MprB* system proposed in Tiwari et al. (2010).

2.1 Structural properties

We note that, by the way that \mathbb{F}^* has been defined, it is dimensionless, and such that for every $t \ge 0$ it holds $0 \le \mathbb{F}^*(t) \le 1$, $\mathbb{F}^* = 0$ means that all RR are unphosphorylated, while $\mathbb{F}^* = 1$ represents the situation with all RR phosphorylated. Clearly, the same holds for \mathbb{S}^* , and hence every state trajectory of the bidimensional system Equations 9, 10 belongs to the feasibility set $\mathcal{C} := \{(\mathbb{F}^*, \mathbb{S}^*): 0 \le \mathbb{F}^* \le 1, \ 0 \le \mathbb{S}^* \le 1\}$.

Proposition 1: The TCS model Equations 9, 10 exhibits a unique equilibrium point $(\mathbb{F}_{eq}^*, \mathbb{S}_{eq}^*)$ within the feasibility set C.

Proof. First, notice that the set \mathcal{C} is positively invariant with respect to systems Equations 9, 10, so that if the state trajectory starts in \mathcal{C} , then it stays in \mathcal{C} for any $t \ge 0$. Positive invariance of the convex and compact set \mathcal{C} ensures that there exists at least one equilibrium point in \mathcal{C} —that is, a limit cycle or at least one stable equilibrium point (Blanchini and Miani, 2015—Theorem 4.21).

We now resort to Bendixon's theorem to rule out the existence of closed orbits.² Note that

$$\begin{split} \frac{df_1}{d\mathbb{r}^*}\left(\mathbb{r}^*,\mathbb{s}^*\right) &= -(\alpha_1 + \alpha_2) - \alpha_3 S_T \left(1 - \mathbb{s}^*\right) - \alpha_4 S_T \mathbb{s}^* < 0, \, \forall \left(\mathbb{r}^*,\mathbb{s}^*\right) \in \mathcal{C} \\ \frac{df_2}{d\mathbb{s}^*}\left(\mathbb{r}^*,\mathbb{s}^*\right) &= -\left(\beta_1 + \beta_2\right) - \beta_3 R_T \left(1 - \mathbb{r}^*\right) - \beta_4 R_T \mathbb{r}^* < 0, \, \forall \left(\mathbb{r}^*,\mathbb{s}^*\right) \in \mathcal{C} \end{split}$$

Hence, $\operatorname{div}(\mathbf{f}) \coloneqq \frac{df_1}{dr^*} + \frac{df_2}{ds^*}$ is not identically zero in any sub-region of the simply connected region \mathcal{C} and does not change sign in \mathcal{C} . Then, by Bendixon's theorem (Sastry, 1999—Theorem 2.7), the set \mathcal{C} contains no closed orbits of system Equations 9, 10.

Finally, we resort to nullcline analysis to prove the uniqueness of steady states. Setting $d\mathbb{P}^*/dt=0$ and $d\mathbb{S}^*/dt=0$ yields the following expressions for \mathbb{P}^* and \mathbb{S}^* nullclines:

$$\mathbb{I}^* = \frac{\alpha_4 S_T \mathbb{S}^* + \alpha_2}{\alpha_1 + \alpha_2 + \alpha_3 S_T (1 - \mathbb{S}^*) + \alpha_4 S_T \mathbb{S}^*} =: g(\mathbb{S}^*)$$
(11)

$$s^* = \frac{\beta_4 R_T \mathbb{F}^* + \beta_2}{\beta_1 + \beta_2 + \beta_3 R_T (1 - \mathbb{F}^*) + \beta_4 R_T \mathbb{F}^*} =: h(\mathbb{F}^*)$$
 (12)

A typical figure of *RR* and *SHK* nullclines is reported in Figure 2. From expression 11, it is easy to obtain $s^* = g^{-1}(\mathfrak{p}^*)$:

$$g^{-1}(\mathbb{F}^*) = \frac{(\alpha_1 + \alpha_2 + \alpha_3 S_T)\mathbb{F}^* - \alpha_2}{\alpha_4 S_T (1 - \mathbb{F}^*) + \alpha_3 S_T \mathbb{F}^*}$$
(13)

We define the function $\Delta(\mathbb{P}^*) \coloneqq h(\mathbb{P}^*) - g^{-1}(\mathbb{P}^*)$ and note that, by the way $\Delta(\mathbb{P}^*)$ has been defined, if $(\mathbb{P}^*_{eq}, \mathbb{S}^*_{eq})$ is an equilibrium point, then $\Delta(\mathbb{P}^*_{eq}) = 0$; *vice versa*, if $\Delta(\mathbb{P}^*) = 0$ then $(\mathbb{P}^*, h(\mathbb{P}^*)) = (\mathbb{P}^*_{eq}, \mathbb{S}^*_{eq})$ is an equilibrium point. It is a matter of computation to verify that $\Delta(\mathbb{P}^*)$ is a rational function— $\Delta(\mathbb{P}^*) = \frac{n(\mathbb{P}^*)}{d(\mathbb{P}^*)}$ and that both the numerator and denominator are polynomials of order 2:

$$\begin{split} n(\mathbb{T}^*) &= \left(\beta_4 R_T \mathbb{T}^* + \beta_2\right) \left(\alpha_4 S_T \left(1 - \mathbb{T}^*\right) + \alpha_3 S_T \mathbb{T}^*\right) \\ &+ - \left(\beta_1 + \beta_2 + \beta_3 R_T \left(1 - \mathbb{T}^*\right) + \beta_4 R_T \mathbb{T}^*\right) \\ &\times \left(\left(\alpha_1 + \alpha_2 + \alpha_3 S_T\right) \mathbb{T}^* - \alpha_2\right) \end{split}$$

$$d\left(\mathbb{r}^{\star}\right) = \left(\beta_{1} + \beta_{2} + \beta_{3}R_{T}\left(1 - \mathbb{r}^{\star}\right) + \beta_{4}R_{T}\mathbb{r}^{\star}\right)\left(\alpha_{4}S_{T}\left(1 - \mathbb{r}^{\star}\right) + \alpha_{3}S_{T}\mathbb{r}^{\star}\right)$$

Note that $d(\mathfrak{r}^*) > 0$ for every $\mathfrak{r}^* \in [0,1]$, and hence $\Delta(\mathfrak{r}^*) = 0$ for some $\mathfrak{r}^* \in [0,1]$ if and only if $n(\mathfrak{r}^*) = 0$ for some $\mathfrak{r}^* \in [0,1]$. Since n(0) > 0 and n(1) < 0, there certainly exists $\mathfrak{r}^*_{eq} \in [0,1]$ such that $n(\mathfrak{r}^*_{eq}) = 0$, and hence $\Delta(\mathfrak{r}^*_{eq}) = 0$ —as already demonstrated, the system admits at least one equilibrium point in \mathcal{C} . On the other hand, since $n(\mathfrak{r}^*)$ is a second-order polynomial, such an \mathfrak{r}^*_{eq} belonging to the interval [0,1] is unique—the system admits a unique equilibrium point \mathcal{C} .

Remark 1: Remark 1. A closed-form expression for the equilibrium point of the TCS can be computed as the unique root in interval [0,1] of the second-order polynomial $n(\mathbb{F}^*)$.

$$\begin{split} \mathbb{F}_{eq}^{\star} &= \alpha_3 \beta_3 R_T S_T - \alpha_4 \beta_4 R_T S_T \pm \\ &\frac{\sqrt{A}}{\left(2\left(\alpha_3 \beta_3 R_T S_T - \alpha_4 \beta_4 R_T S_T + \alpha_1 \beta_3 R_T + \alpha_2 \beta_3 R_T - \alpha_1 \beta_4 R_T - \alpha_2 \beta_4 R_T\right)\right)} \end{split}$$

with. $A = (-\alpha_3\beta_3R_TS_T + \alpha_4\beta_4R_TS_T - \alpha_1\beta_3R_T - 2\alpha_2\beta_3R_T + \alpha_2\beta_4R_T - \alpha_3\beta_1S_T - \alpha_4\beta_2S_T - \alpha_1\beta_1 - \alpha_2\beta_1 - \alpha_1\beta_2 - \alpha_2\beta_2)^2 - 4(\alpha_2\beta_3R_T + \alpha_4\beta_2S_T + \alpha_2\beta_1 + \alpha_2\beta_2)(\alpha_3\beta_3R_TS_T - \alpha_4\beta_4R_TS_T + \alpha_1\beta_3R_T + \alpha_2\beta_3R_T - \alpha_1\beta_4R_T - \alpha_2\beta_4R_T) + \alpha_1\beta_3R_T + 2\alpha_2\beta_3R_T - \alpha_2\beta_4R_T + \alpha_3\beta_1S_T + \alpha_4\beta_2S_T + \alpha_1\beta_1 + \alpha_2\beta_1 + \alpha_1\beta_2 + \alpha_2\beta_2)$

Proposition 1 states that all trajectories with initial conditions in \mathcal{C} converge to a unique equilibrium point $(\mathbb{F}_{eq}^*, \mathbb{S}_{eq}^*) \in \mathcal{C}$. This means

² Since every limit cycle is a closed orbit, ruling out the existence of closed orbits automatically excludes the existence of limit cycles.

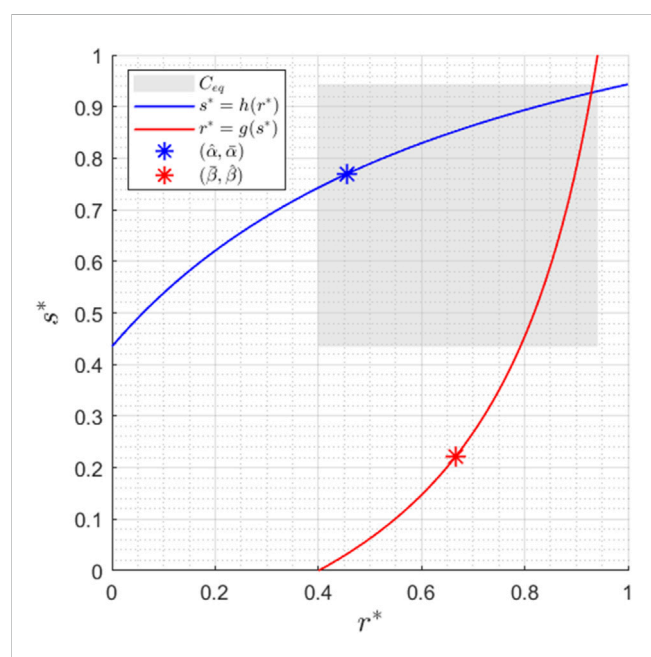


FIGURE 2 Nullclines for $\alpha_1=0.5$, $\alpha_2=1$, $\alpha_3=1$, $\alpha_4=7$, $\beta_1=0.3$, $\beta_2=1$, $\beta_3=1$, $\beta_4=4$, $R_T=1$, and $S_T=1$. The C_{eq} region corresponds to the subregion where the equilibrium point is located, as detailed in Proposition 2.

that, independently of the initial relative amounts of phosphorylated and unphosphorylated proteins, the proportion of phosphorylated to total RR will asymptotically equal \mathbb{F}_{eq}^* , while the proportion of phosphorylated to total SHK will asymptotically tend to \mathbb{S}_{eq}^* . The following proposition identifies a subregion $\mathcal{C}_{eq} \subsetneq \mathcal{C}$ where the equilibrium point is located and hence provides upper and lower bounds to the phosphorylation levels \mathbb{F}_{eq}^* and \mathbb{S}_{eq}^* asymptotically reached by the TCS.

Proposition 2: Consider the TCS described by models Equations 9, 10. The unique equilibrium point of the system, denoted by $(\mathbb{F}_{eq}^*, \mathbb{S}_{eq}^*)$, belongs to the subregion

$$\mathcal{C}_{eq} \coloneqq \{(\mathbb{F}^\star, \mathbb{S}^\star) \colon \mathbb{F}^\star_{min} \leq \mathbb{F}^\star \leq \mathbb{F}^\star_{max} \,, \ \mathbb{S}^\star_{min} \leq \mathbb{S}^\star \leq \mathbb{S}^\star_{max} \,\} \subsetneq \mathcal{C},$$

where

$$\begin{split} \mathbb{F}_{min}^{\star} \colon &= \frac{\alpha_2}{\alpha_1 + \alpha_2 + \alpha_3 S_T}, \ \mathbb{F}_{max}^{\star} \colon &= \frac{\alpha_4 S_T + \alpha_2}{\alpha_1 + \alpha_2 + \alpha_4 S_T}, \\ \mathbb{S}_{min}^{\star} \colon &= \frac{\beta_2}{\beta_1 + \beta_2 + \beta_3 R_T}, \ \mathbb{S}_{max}^{\star} \colon &= \frac{\beta_4 R_T + \beta_2}{\beta_1 + \beta_2 + \beta_4 R_T} \end{split}$$

Proof. Consider the expression for RR nullcline Equation 11 and note that

$$\frac{\partial g}{\partial s^*}(s^*) = \frac{S_T(\alpha_1 \alpha_4 + \alpha_4 \alpha_3 S_T + \alpha_2 \alpha_3)}{(\alpha_1 + \alpha_2 + \alpha_3 S_T (1 - s^*) + \alpha_4 S_T s^*)^2} > 0 \quad \text{for everys}^* \in [0, 1],$$

and hence \mathbb{r}^* is strictly monotonically increasing in \mathbb{s}^* . The bounds on \mathbb{r}_{eq}^* then follow from

$$g(0) = \frac{\alpha_2}{\alpha_1 + \alpha_2 + \alpha_3 S_T} =: \mathbb{F}_{min}^*, \text{ and}$$

$$g(1) = \frac{\alpha_4 S_T + \alpha_2}{\alpha_1 + \alpha_2 + \alpha_4 S_T} =: \mathbb{F}_{max}^*,$$

Analogous computations on SHK nullcline Equation 12 lead to upper and lower bounds on \mathfrak{S}_{eq}^* .

The set C_{eq} is reported in Figure 2 for the set of parameters considered. We conclude this section with the following Lemma, which will be useful for subsequent derivations (see again Figure 2).

Lemma 1: Consider the TCS described by models Equations 9, 10, and define

$$\bar{\alpha} : = \frac{\alpha_2 \alpha_3}{\alpha_2 \alpha_3 + \alpha_1 \alpha_4} \hat{\alpha} : = \frac{\alpha_2}{\alpha_1 + \alpha_2}$$

$$\bar{\beta} : = \frac{\beta_2 \beta_3}{\beta_2 \beta_3 + \beta_1 \beta_4} \hat{\beta} : = \frac{\beta_2}{\beta_1 + \beta_2}$$

Then, RR nullcline Equation 11 always passes through $(\bar{\alpha}, \hat{\alpha}) - g(\bar{\alpha}) = \hat{\alpha}$ —while SHK nullcline Equation 12 always passes through $(\bar{\beta}, \hat{\beta}) - h(\bar{\beta}) = \hat{\beta}$.

This behavior can also be observed in Figure 3, where the dotted lines indicate the nullclines associated with higher values of R_T and S_T , while the dashed lines are the nullclines obtained with lower values of R_T and S_T , as described in the caption.

Since verifying that $g(\bar{\alpha}) = \hat{\alpha}$ and $h(\bar{\beta}) = \hat{\beta}$ is just a matter of computation, the proof of Lemma 1 is omitted.

At this point, two observations are in order. First, the dimensionless values \mathbb{F}_{eq}^* and \mathbb{S}_{eq}^* depend on the total amounts of RR and SHK proteins present within the system (recall that, due to time scale separation, so far we have assumed that the quantities R_T and S_T are constant). In other words, \mathbb{F}_{eq}^* and \mathbb{S}_{eq}^* are continuous functions of R_T and $S_T - \mathbb{F}_{eq}^* = \mathbb{F}_{eq}^*$ (R_T, S_T) and $\mathbb{S}_{eq}^* = \mathbb{S}_{eq}^*$ (R_T, S_T). The second observation is that uniform monotonicity of \mathbb{F}_{eq}^* (R_T, S_T) and \mathbb{S}_{eq}^* (R_T, S_T) with respect to their arguments is not guaranteed. Depending on the values taken by the system parameters, equilibrium \mathbb{F}_{eq}^* might decrease with R_T when R_T belongs to a specific interval, and increase with R_T when it belongs to a different interval.

3 Relative concentrations

3.1 Low vs high R_T concentration

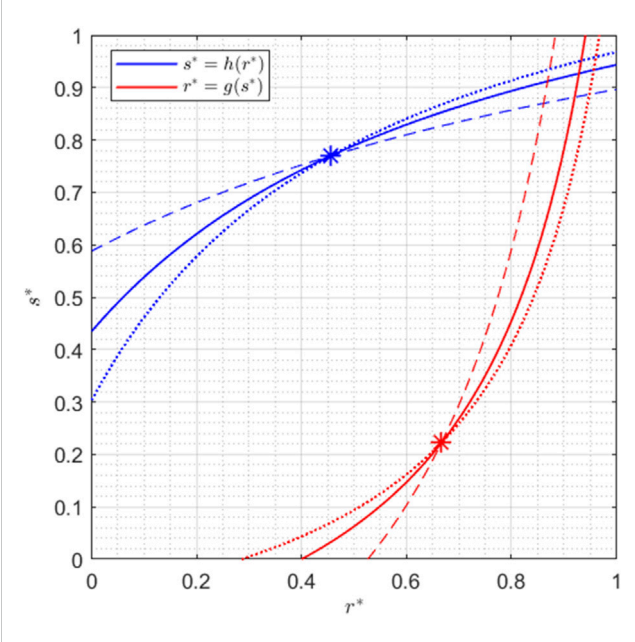
In this section, we assume that R_T and S_T are independent.

Proposition 3: (Low R_T concentration.) Consider the TCS described by models Equations 9, 10 and let the total SHK concentration S_T be arbitrary but fixed. When the total RR concentration is extremely low—that is, for $R_T \to 0$ —the equilibrium point asymptotically reached by the system is given by $(\mathbb{F}_{eq}^*, \mathbb{S}_{eq}^*) = (g(\hat{\beta}), \hat{\beta})$.

Proof. By taking the limit for $R_T \to 0$ of the function $h(\mathbb{F}^*)$ defined in Equation 12 and representing SHK nullcline,³ it can be seen that $\mathbb{S}_{eq}^* = \hat{\beta}$. The result then follows by plugging \mathbb{S}_{eq}^* into RR-nullcine Equation 11.

³ An equivalent way to see that $s_{eq}^* = \hat{\beta}$ when $R_T \to 0$ is noticing that in this case both s_{min}^* and s_{max}^* tend to $\beta_2/(\beta_1 + \beta_2) = \hat{\beta}$, and hence the subregion \mathcal{C}_{eg} reduces to a line.

10.3389/fsysb.2025.1693064 Zorzan et al.



Nullclines for $\alpha_1 = 0.5$, $\alpha_2 = 1$, $\alpha_3 = 1$, $\alpha_4 = 7$, $\beta_1 = 0.3$, $\beta_2 = 1$, $\beta_3 = 1$, and $\beta_4 = 4$. The solid lines have $R_T = 1$ and $S_T = 1$ as in Figure 2; the dashed lines are obtained with $R_T = 0.4$ and $S_T = 0.4$; the dotted lines with $R_T = 2$ and $S_T = 2$

Proposition 4: (High R_T concentration.) Consider the TCS described by models Equations 9, 10 and let the total SHK concentration S_T be arbitrary but fixed. When the total RR concentration is extremely high—that is, for $R_T \to +\infty$ —the equilibrium point asymptotically reached by the system is $(\mathbb{F}_{hR}^*, h(\mathbb{F}_{hR}^*))$, with \mathbb{F}_{hR}^* being the (unique) solution in the interval [0,1] of the quadratic equation $\mathbf{A} (\mathbf{r}^*)^2 + \mathbf{B} \mathbf{r}^* + \mathbf{C} = 0$, where

A: =
$$(\alpha_1 + \alpha_2 + \alpha_3 S_T)\beta_3 - (\alpha_2 + \alpha_4 S_T)\beta_4 - \alpha_1 \beta_4$$

B: = $-(\alpha_1 + \alpha_2 + \alpha_3 S_T)\beta_3 + (\alpha_2 + \alpha_4 S_T)\beta_4 - \alpha_2 \beta_3$
C: = $\alpha_2 \beta_3$

More specifically, $\mathbb{F}_{hR}^* = (-\mathbf{B} - \sqrt{\mathbf{B}^2 - 4\mathbf{AC}})/(2\mathbf{A})$.

Proof. Note that when $R_T \to +\infty$, the upper and lower bounds on s_{eq}^* are given by $s_{min}^* = 0$ and $s_{max}^* = 1$, respectively, and hence do not provide any useful information. Taking the limit for $R_T \rightarrow +$ ∞ of RR and SHK nullclines Equations 13, 12 yields

$$\lim_{R_T \to +\infty} g^{-1}(\mathbb{P}^*) = \frac{(\alpha_1 + \alpha_2 + \alpha_3 S_T)\mathbb{P}^* - \alpha_2}{\alpha_4 S_T (1 - \mathbb{P}^*) + \alpha_3 S_T \mathbb{P}^*}$$

$$\lim_{R_T \to +\infty} h(\mathbb{P}^*) = \frac{\beta_4 \mathbb{P}^*}{\beta_4 \mathbb{P}^* + \beta_3 (1 - \mathbb{P}^*)}$$

Solving for $\lim_{R_T\to+\infty}g^{-1}(\mathfrak{r}^*)=\lim_{R_T\to+\infty}h(\mathfrak{r}^*)$ leads to the quadratic equation $\mathbf{A}(\mathbf{r}^*)^2 + \mathbf{B}\mathbf{r}^* + \mathbf{C} = 0$. The result now follows upon noting that if $(\alpha_1 + \alpha_2 + \alpha_3 S_T)\beta_3 > (\alpha_1 + \alpha_2 + \alpha_4 S_T)\beta_4$, then A > 0 and B < 0, otherwise A < 0; by Descartes' rule of signs, the quadratic equation has a unique positive solution.

Corollary 1: Consider the TCS described by models Equations 9, 10 and let the total SHK concentration S_T be arbitrary but fixed. Assuming the total RR concentration to be very high—that is, $R_T \rightarrow + \infty$ —then if $\beta_3 \neq 0$ and $\beta_4 = 0$, the equilibrium point asymptotically reached by the system is $(\mathbb{F}_{min}^*, 0)$; if $\beta_3 = 0$ and $\beta_4 \neq 0$, the equilibrium point is $(\mathbb{F}_{max}^*, 1)$.

Proof. Consider the scenario with $\beta_3 \neq 0$ and $\beta_4 = 0$ and note that in this case, $\mathbb{S}_{max}^* = \frac{\beta_2}{\beta_1 + \beta_2}$. Taking the limit for $R_T \to +\infty$ of SHK nullcline (12) yields

$$\mathbb{S}_{eq}^{\star} = \lim_{R_T \to +\infty} \frac{\beta_2}{\beta_1 + \beta_2 + \beta_3 R_T (1 - \mathbb{F}^{\star})} = 0, \qquad \mathbb{S}_{min}^{\star} = 0.$$

Then, from *RR* nullcline Equation 11, we have $\mathbb{F}_{eq}^* = g(\mathbb{S}_{eq}^*) = \mathbb{F}_{min}^{*}$. The proof for the case $\beta_3 = 0$ and $\beta_4 \neq 0$ follows the same line and is hence omitted.

Figure 4 reports, for an illustrative set of parameters, equilibrium values \mathbb{F}_{eq}^* and \mathbb{S}_{eq}^* as a function of R_T .

By symmetry, analogous results on the equilibrium point hold when the SHK total amount is extremely low or extremely high— $S_T \to 0$ or $S_T \to +\infty$.

3.2 Uniform monotonicity of the equilibrium with respect to R_T and S_T

We now consider small perturbations of R_T and S_T concentrations and investigate their effects on the equilibrium point $(\mathbb{F}_{eq}^*, \mathbb{S}_{eq}^*)$.

We assume first that S_T is constant and consider small perturbations of R_T . The equilibrium values continuously depend on R_T —that is, $(\mathfrak{r}_{eq}^*, \mathfrak{s}_{eq}^*) = (g(\mathfrak{s}_{eq}^*, R_T), h(\mathfrak{r}_{eq}^*, R_T))$ —and this dependence is quantitatively described by

$$\frac{\partial \mathbb{F}_{eq}^{\star}}{\partial R_T} = \frac{\partial g}{\partial \mathbb{S}^{\star}} \frac{\partial \mathbb{S}_{eq}^{\star}}{\partial R_T}$$
 (14)

$$\frac{\partial s_{eq}^*}{\partial R_T} = \frac{\partial h}{\partial v^*} \frac{\partial v_{eq}^*}{\partial R_T} + \frac{\partial h}{\partial R_T}$$
(15)

Conversely, if we assume that total concentration R_T is constant while S_T slowly varies, we have

$$\frac{\partial \mathbb{I}_{eq}^{\star}}{\partial S_{T}} = \frac{\partial g}{\partial s^{\star}} \frac{\partial s_{eq}^{\star}}{\partial S_{T}} + \frac{\partial g}{\partial S_{T}}$$
(16)

$$\frac{\partial \mathbb{S}_{eq}^{\star}}{\partial S_{T}} = \frac{\partial h}{\partial \mathbb{F}^{\star}} \frac{\partial \mathbb{F}_{eq}^{\star}}{\partial S_{T}}$$
 (17)

Putting together Equations 14-17 and solving for the variation of equilibria with respect to R_T and S_T , we obtain

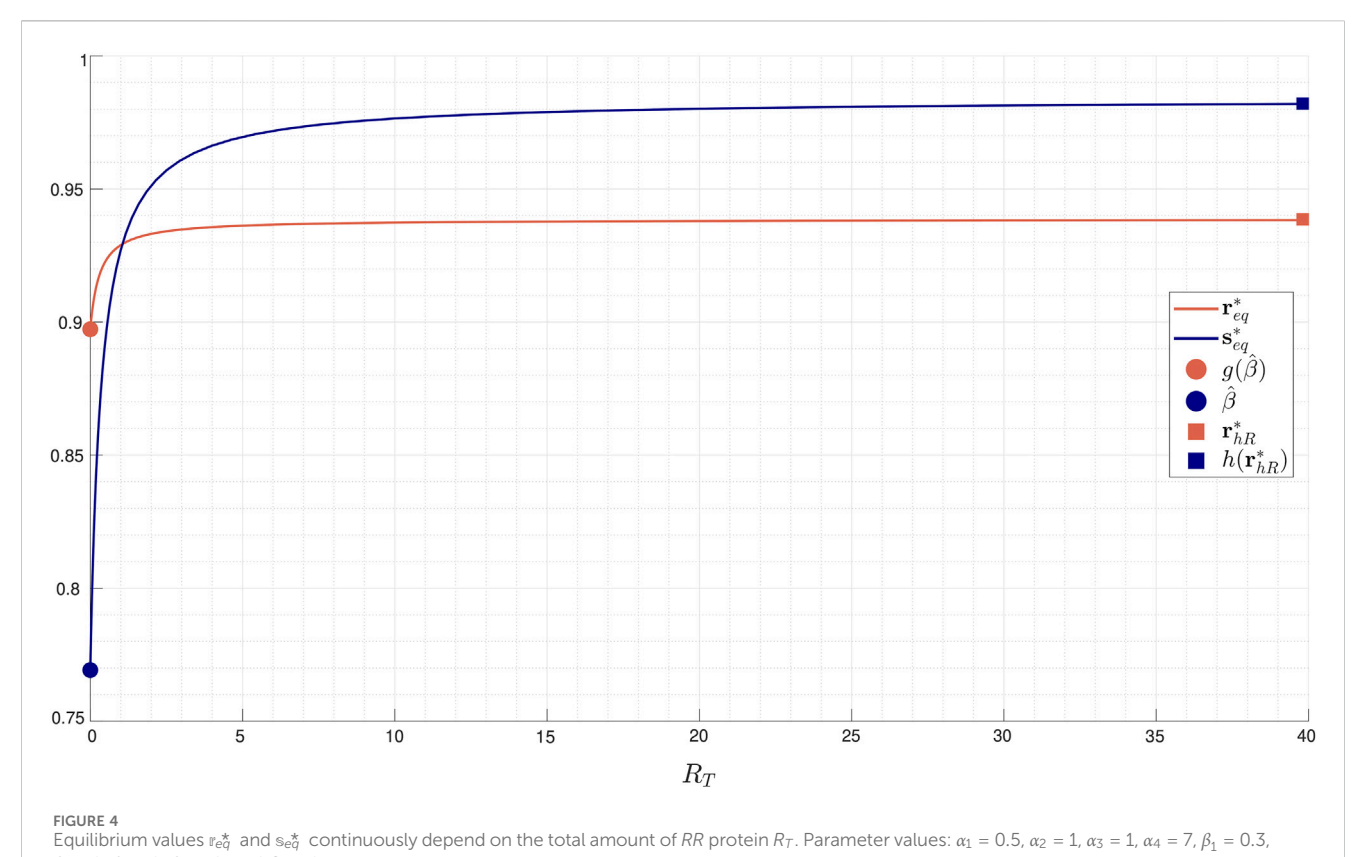
$$\frac{\partial \mathbb{F}_{eq}^{\star}}{\partial R_{T}} = \frac{\frac{\partial h}{\partial R_{T}} \frac{\partial g}{\partial s^{\star}}}{1 - \frac{\partial h}{\partial r} \frac{\partial g}{\partial s^{\star}}} \qquad \frac{\partial \mathbb{S}_{eq}^{\star}}{\partial R_{T}} = \frac{\frac{\partial h}{\partial R_{T}}}{1 - \frac{\partial h}{\partial r} \frac{\partial g}{\partial s^{\star}}} \qquad (18)$$

$$\frac{\partial \mathbb{F}_{eq}^{\star}}{\partial S_{T}} = \frac{\frac{\partial g}{\partial S_{T}}}{1 - \frac{\partial h}{\partial r} \frac{\partial g}{\partial s^{\star}}} \qquad \frac{\partial \mathbb{S}_{eq}^{\star}}{\partial S_{T}} = \frac{\frac{\partial g}{\partial S_{T}} \frac{\partial h}{\partial r^{\star}}}{1 - \frac{\partial h}{\partial r} \frac{\partial g}{\partial s^{\star}}} \qquad (19)$$

$$\frac{\partial v_{eq}^*}{\partial S_T} = \frac{\frac{\partial g}{\partial S_T}}{1 - \frac{\partial h}{\partial r^*} \frac{\partial g}{\partial s^*}} \qquad \frac{\partial s_{eq}^*}{\partial S_T} = \frac{\frac{\partial g}{\partial S_T} \frac{\partial h}{\partial r^*}}{1 - \frac{\partial h}{\partial r^*} \frac{\partial g}{\partial s^*}}$$
(19)

Proposition 5: Consider the TCS described by model Equations 9, 10, and let $(\mathbb{F}_{eq}^{\star}, \mathbb{S}_{eq}^{\star})$ denote the (unique) equilibrium point of the system. The equilibrium values $\mathbb{F}_{eq}^* = \mathbb{F}_{eq}^* (R_T, S_T)$ and $\mathbb{S}_{eq}^* = \mathbb{F}_{eq}^* (R_T, S_T)$ $s_{ea}^{\star}(R_T, S_T)$ are:

⁴ Alternatively, the result directly follows from Proposition 4 with $\beta_3 = 0$.



- $\beta_2 = 1$, $\beta_3 = 1$, $\beta_4 = 4$, and $S_T = 1$.
- i) monotonically increasing in their arguments if $\hat{\alpha} > \bar{\beta}$ and $\hat{\beta} > \bar{\alpha}$;
- ii) monotonically decreasing in their arguments if $\hat{\alpha} < \overline{\beta}$ and $\hat{\beta} < \overline{\alpha}$. Proof. Observe that

$$\frac{\partial h}{\partial \mathbb{F}^*} = \frac{R_T \left(\beta_1 \beta_4 + \beta_4 \beta_3 R_T + \beta_3 \beta_2\right)}{\left(\beta_1 + \beta_2 + \beta_3 R_T \left(1 - \mathbb{F}^*\right) + \beta_4 R_T \mathbb{F}^*\right)^2} \ge 0 \quad \text{for every } \mathbb{F}^* \in [0, 1],$$

and by symmetry, also $\frac{\partial g}{\partial s^*} \ge 0$ for every $s^* \in [0,1]$. Moreover, recall that the function $\Delta(\mathfrak{r}^*) := h(\mathfrak{r}^*) - g^{-1}(\mathfrak{r}^*)$ is such that $\Delta(0) > 0$ and $\Delta(1) < 0$ (see proof of Theorem 1), and hence at the equilibrium $\frac{\partial \Delta}{\partial s^*} = \frac{\partial h}{\partial r^*} - \frac{\partial g^{-1}}{\partial r^*} < 0 - \frac{\partial h}{\partial r^*} < \frac{\partial g^{-1}}{\partial r^*}$. This, in turn, implies that

$$0 < \frac{\frac{\partial h}{\partial \mathbb{I}^*}}{\frac{\partial g^{-1}}{\partial \mathbb{I}^*}} = \frac{\partial h}{\partial \mathbb{I}^*} \frac{\partial g}{\partial \mathbb{S}^*} < 1$$

Then, the sign of the partial derivatives Equations 18, 19 are solely determined by $\frac{\partial h}{\partial R_T}$ and $\frac{\partial g}{\partial S_T}$ since all other terms are always nonnegative. It is a matter of computation to verify that

$$\frac{\partial h}{\partial R_T} = \frac{\left(\beta_1\beta_4 + \beta_2\beta_3\right)\mathbb{r}^* - \beta_2\beta_3}{\left(\beta_1 + \beta_2 + \beta_3R_T\left(1 - \mathbb{r}^*\right) + \beta_4R_T\mathbb{r}^*\right)^2},$$

and hence at equilibrium $\operatorname{sign}(\frac{\partial h}{\partial R_T}) = \operatorname{sign}(\mathbb{F}_{eq}^* - \bar{\beta})$. Exploiting again the symmetry of the system, we can claim that $\operatorname{sign}(\frac{\partial g}{\partial S_T}) = \operatorname{sign}(\mathbb{S}_{eq}^* - \bar{\alpha})$. Hence, provided that \mathbb{F}_{eq}^* (\mathbb{S}_{eq}^*) is greater than $\bar{\beta}$ (respectively, $\bar{\alpha}$), both \mathbb{F}_{eq}^* and \mathbb{S}_{eq}^* are monotonically increasing functions of R_T (respectively, S_T). Similarly, provided that \mathbb{F}_{eq}^* (\mathbb{S}_{eq}^*) is smaller than $\bar{\beta}$ (respectively,

 $\bar{\alpha}$), both \mathbb{F}_{eq}^* and \mathbb{S}_{eq}^* are monotonically decreasing functions of R_T (respectively, S_T). It is clear from Figure 2 that when $\hat{\alpha} > \bar{\beta}$ and $\hat{\beta} > \bar{\alpha}$, the equilibrium values necessarily satisfy the inequalities $\mathbb{F}_{eq}^* > \bar{\beta}$ and $\mathbb{S}_{eq}^* > \bar{\alpha}$, and the thesis follows.

Remark 2: The conditions on the system parameters provided by proposition 5 are sufficient (but not necessary) for uniform monotonicity of the equilibrium concerning total concentrations R_T and S_T . It is worth noticing that such a result is extremely powerful; its strength resides in the fact that it does not depend on the specific form of the functions R_T and S_T (provided they are monotone). More specifically, let $R_T = f_R(u_{ext})$ and $S_T = f_S(u_{ext})$, where u_{ext} is an external signal and f_R and f_S are monotone functions. Then, $u_{ext} = f_R^{-1}(R_T)$, and the relationship between S_T and R_T is given by $S_T = f_S \circ f_R^{-1}(R_T)$ (note that the composite function $f_S \circ f_R$ is itself monotone). Proposition 5 states that if $\hat{\alpha} > \bar{\beta}$ and $\hat{\beta} > \bar{\alpha}$, monotonicity of the equilibrium with respect to R_T and S_T is ensured independently on the specific form of the monotone functions f_R and f_S . If the previous conditions are not satisfied, uniform monotonicity is not guaranteed.

We now focus on the case where a proportionality relationship among R_T and S_T can be assumed: $S_T = f_S \circ f_R(R_T) = \lambda R_T$. Note that this is a perfectly reasonable assumption when phosphorylated RR activates the transcription of both its gene and the gene encoding its partner SHK—see, for example, the mathematical description of the MprA/MprB two-component system adopted in (Tiwari et al., 2010).

Theorem 1: Consider the TCS described by models Equations 9, 10, and assume that total RR and SHK concentrations are related by $S_T = \lambda R_T$, where $\lambda > 0$ is a fixed (not necessarily known) proportionality coefficient. When the total RR concentration is extremely high—that is, for $R_T \to + \infty$ —the (unique) equilibrium point asymptotically reached by the system is

$$\left(\mathbb{F}_{eq}^{\star}, \mathbb{S}_{eq}^{\star}\right) = \left\{ \begin{array}{ll} (0,0), & \text{if } \frac{\alpha_{3}\beta_{3}}{\alpha_{4}\beta_{4}} > 1 \\ \\ (1,1), & \text{if } \frac{\alpha_{3}\beta_{3}}{\alpha_{4}\beta_{4}} < 1 \end{array} \right.$$

Proof. Compute the limit for $R_T \to +\infty$ of RR and SHK nullclines Equations 11, 12:

$$\mathbb{F}^* = \lim_{R_T \to +\infty} g(\mathbb{S}^*, \lambda R_T) = \frac{\alpha_4 \mathbb{S}^*}{\alpha_3 + (\alpha_4 - \alpha_3) \mathbb{S}^*}, \text{ for every } \lambda > 0$$
 (20)

$$\mathbb{S}^* = \lim_{R_T \to +\infty} h(\mathbb{I}^*, R_T) = \frac{\beta_4 \mathbb{I}^*}{\beta_3 + (\beta_4 - \beta_3) \mathbb{I}^*}$$
(21)

From expression Equation 21, it is easy to obtain

$$\mathbb{F}^* = h^{-1}(\mathbb{S}^*) = \frac{\beta_3 \mathbb{S}^*}{\beta_4 + (\beta_3 - \beta_4) \mathbb{S}^*}$$

Substituting the previous expression into Equation 20 and solving for s* yields the following quadratic equation:

$$(s^*)^2 \{ (\alpha_4 \beta_4 - \alpha_3 \beta_3) s^* + (\alpha_3 \beta_3 - \alpha_4 \beta_4) \} = 0$$

Then, the only two possible equilibrium points are $(\mathbb{F}_{eq}^*, \mathbb{S}_{eq}^*) = (0,0)$ and $(\mathbb{F}_{eq}^*, \mathbb{S}_{eq}^*) = (1,1)$. To determine which is the right solution, we need to resort to the intersection condition $\frac{\partial h}{\partial x^*} \frac{\partial g}{\partial s^*} < 1$ (see the proof of Proposition 5). Indeed, it is straightforward to verify that

$$\lim_{R_T \to +\infty} \frac{\partial h}{\partial \mathbb{P}^*} = \frac{\beta_3 \beta_4}{(\beta_3 + (\beta_4 - \beta_3)\mathbb{P}^*)^2}$$

$$\lim_{R_T \to +\infty} \frac{\partial g}{\partial s^*} = \frac{\alpha_3 \alpha_4}{(\alpha_3 + (\alpha_4 - \alpha_3)s^*)^2},$$

and hence

$$\begin{split} \frac{\partial h}{\partial \mathbf{r}^*} \frac{\partial g}{\partial \mathbf{s}^*} \big|_{(\mathbf{r}^*,\mathbf{s}^*)=(0,0)} &= \frac{\beta_4}{\beta_3} \frac{\alpha_4}{\alpha_3} \\ \frac{\partial h}{\partial \mathbf{r}^*} \frac{\partial g}{\partial \mathbf{s}^*} \big|_{(\mathbf{r}^*,\mathbf{s}^*)=(1,1)} &= \frac{\beta_3}{\beta_4} \frac{\alpha_3}{\alpha_4}, \end{split}$$

which uniquely determines the limiting equilibrium pair once the quantity $\frac{\beta_4}{\beta_3} \frac{\alpha_4}{\alpha_3}$ is known.

Remark 3: The previous result does not require knowledge of the value assumed by the proportionality coefficient λ ; we just need to know that a proportionality coefficient continuously relates R_T and S_T

4 Absolute concentrations

We have thus far analyzed the properties (asymptotic behavior and monotonicity) of *relative* concentrations: of the ratio between phosphorylated and unphosphorylated protein concentrations. A fundamental and crucial point is that these properties do not necessarily hold for absolute concentrations too: the fact that the relative concentration \mathbb{F}_{eq}^* tending to 0 does not imply that absolute concentration r_{eq}^* tends to 0; similarly, uniform monotonicity of \mathbb{F}_{eq}^* for R_T does not imply uniform monotonicity of r^* to R_T . To understand this point, note that the relative concentration \mathbb{F}_{eq}^* tends to 0 when total RR concentration asymptotically grows to infinity (i.e., $R_T \to +\infty$) and r^* asymptotically approaches a given saturation level $r_{eq}^* \neq 0$. Regarding monotonicity, since $r^* = \mathbb{F}^* R_T$, it holds that

$$\frac{\partial r^*}{\partial R_T} = \frac{\partial \mathbb{I}^*}{\partial R_T} R_T + \mathbb{I}^*$$

It is clear that if \mathbb{F}_{eq}^* is a monotonically increasing function of R_T (namely, $\frac{\partial \mathbb{F}^*}{\partial R_T} > 0$), so is r_{eq}^* . On the contrary, if \mathbb{F}_{eq}^* is a monotonically decreasing function of R_T , and hence $\frac{\partial \mathbb{F}^*}{\partial R_T} < 0$; monotonicity of r_{eq}^* with respect to R_T is not guaranteed.

In the following, we analyze the asymptotic behavior of absolute concentrations r_{eq}^* and s_{eq}^* when R_T grows to infinity, under the assumption that RR and SHK total concentrations are linearly related with the proportionality coefficient $\lambda - S_T = \lambda R_T$.

Theorem 2: Consider the TCS described by models Equations 9, 10 and assume that the total RR and SHK concentrations are linearly related by $S_T = \lambda R_T$, where $\lambda > 0$ is a fixed proportionality coefficient. When total RR concentration is sufficiently high—that is, for $R_T \to +\infty$, RR and SHK—then absolute concentrations asymptotically approach the equilibrium values:

$$r_{eq}^{\star} = \frac{\alpha_2 \beta_3 + \lambda \alpha_4 \beta_2}{\lambda (\alpha_3 \beta_3 - \alpha_4 \beta_4)}$$
 $s_{eq}^{\star} = \frac{\alpha_2 \beta_4 + \lambda \alpha_3 \beta_2}{\alpha_3 \beta_3 - \alpha_4 \beta_4}$

respectively

Proof. We claim that for a sufficiently high R_T , absolute equilibrium concentrations r_{eq}^* and s_{eq}^* asymptotically approach saturation levels ρ and σ :

$$\lim_{R_T \to +\infty} \left\{ \mathbb{F}_{eq}^{\star} \left(R_T, \lambda R_T \right) \cdot R_T \right\} = \rho,$$

$$\lim_{R_T \to +\infty} \left\{ \mathbb{S}_{eq}^{\star} \left(R_T, \lambda R_T \right) \cdot \lambda R_T \right\} = \sigma$$

We now seek to determine the values ρ and $\sigma.$ First, we note that

$$\begin{split} & \rho = \lim_{R_T \to +\infty} g \Big(\mathbb{S}_{eq}^{\star} \left(R_T, \lambda R_T \right), \lambda R_T \Big) \cdot R_T \\ & = \lim_{R_T \to +\infty} \frac{\alpha_4 \lambda R_T \mathbb{S}_{eq}^{\star} \left(R_T, \lambda R_T \right) + \alpha_2}{\alpha_1 + \alpha_2 + \alpha_3 \lambda R_T \Big(1 - \mathbb{S}_{eq}^{\star} \left(R_T, \lambda R_T \right) \Big) + \alpha_4 \lambda R_T \mathbb{S}_{eq}^{\star} \left(R_T, \lambda R_T \right)} \cdot R_T \\ & = \lim_{R_T \to +\infty} \frac{\alpha_4 \sigma + \alpha_2}{\alpha_1 + \alpha_2 + \alpha_3 \lambda R_T + (\alpha_4 - \alpha_3) \sigma} \cdot R_T \\ & = \frac{\alpha_4 \sigma + \alpha_2}{\lambda \alpha_3} \end{split}$$

Analogously, the limit of s_{eq}^* for $R_T \to +\infty$ can be computed as

$$\begin{split} \sigma &= \lim_{R_T \to +\infty} h \Big(\mathbb{T}_{eq}^{\star} \left(R_T, \lambda R_T \right), \lambda R_T \Big) \cdot \lambda R_T \\ &= \lim_{R_T \to +\infty} \frac{\beta_4 R_T \mathbb{T}_{eq}^{\star} \left(R_T, \lambda R_T \right) + \beta_2}{\beta_1 + \beta_2 + \beta_3 R_T \Big(1 - \mathbb{T}_{eq}^{\star} \left(R_T, \lambda R_T \right) \Big) + \beta_4 R_T \mathbb{T}_{eq}^{\star} \left(R_T, \lambda R_T \right)} \cdot \lambda R_T \\ &= \lim_{R_T \to +\infty} \frac{\beta_4 \rho + \beta_2}{\beta_1 + \beta_2 + \beta_3 R_T + \left(\beta_4 - \beta_3 \right) \rho} \cdot \lambda R_T \\ &= \frac{\left(\beta_4 \rho + \beta_2 \right) \lambda}{\beta_3} \end{split}$$

Therefore, we need to solve the linear system:

$$\begin{cases} \rho \lambda \alpha_3 = \alpha_4 \sigma + \alpha_2 \\ \sigma \beta_3 = (\beta_4 \rho + \beta_2) \lambda \end{cases}$$

Solving for ρ and σ yields

$$\rho = \frac{\alpha_2\beta_3 + \lambda\alpha_4\beta_2}{\lambda\left(\alpha_3\beta_3 - \alpha_4\beta_4\right)}, \qquad \sigma = \frac{\alpha_2\beta_4 + \lambda\alpha_3\beta_2}{\alpha_3\beta_3 - \alpha_4\beta_4},$$

Thus, the proof is concluded.

It follows from Theorem 2 that for sufficiently high R_T , while the amount of phosphorylated SHK increases with λ , the amount of phosphorylated RR is a decreasing function of λ , such that

$$r_{eq}^* = \frac{\frac{1}{\lambda}\alpha_2\beta_3 + \alpha_4\beta_2}{\alpha_3\beta_3 - \alpha_4\beta_4} \tag{22}$$

5 Discussion

A distinguishing feature of the proposed TCS mathematical model is that it accounts for a variety of reactions, including *RR* phosphorylation and dephosphorylation through external (exogenous) pathways, *SHK* autophosphorylation and autodephosphorylation, *RR* phosphorylation via phosphotransfer from *SHK*, and *RR* dephosphorylation via *SHK*. Of course, by setting 0 for one or more parameters, the model can be tailored to specific two-component systems (TCSs) and/or situations in which some of the previous reactions are negligible.

One of the best characterized examples of TCS is the EnvZ/ OmpR system in Escherichia coli, which responds to changes in environmental osmolality by regulating the expression of the outer membrane porins OmpF and OmpC. As in many TCSs, EnvZ is a bifunctional sensor histidine kinase, meaning that it phosphorylates and dephosphorylates the response regulator OmpR. Batchelor and Goulian (2003) proposed a mathematical model of the EnvZ/OmpR TCS and experimentally tested the model's predictions. Their main finding was that for sufficiently high amounts of OmpR, when total EnvZ in the cell is much less abundant than total OmpR⁵, the steadystate level of phosphorylated OmpR is robust (insensitive) to fluctuations in EnvZ and OmpR concentrations. This model accounts for the autokinase, phosphotransfer, and phosphatase activities of EnvZ and neglects the exogenous phosphorylation and dephosphorylation of OmpR. Casting such a scenario into our mathematical framework means setting α_2 and β_4 to 0. Theorem 2 then implies that the equilibrium absolute concentration for *OmpR* is given by $r_{eq}^* = \frac{\alpha_4 \beta_2}{\alpha_3 \beta_3}$, and hence, consistent with Batchelor and Goulian (2003), does not depend on EnvZ total concentration. However, our model shows that if an exogenous RR phosphorylation flux is present ($\alpha_2 \neq 0$), the previous result fails; when an external pathway for OmpR phosphorylation is present, the steady-state concentration of phosphorylated OmpR is (higher and) decreasing with λ (see Equation 22). Notably, Batchelor and Goulian (2003) predicted, via theoretical analysis and experimental verification with fluorescent reporter strains, that when condition $S_T \ll R_T$ does not hold, the steady-state value of OmpR-P decreases with increasing total EnvZ concentration. This is consistent with our theoretical results, which also shed light on the role of an EnvZ-independent mechanism for OmpR phosphorylation.

Furthermore, our analysis allows the characterization of the steady-state concentration of the histidine kinase: $s_{eq}^* = \lambda \frac{\beta_2}{\beta_3}$ (recall that $\beta_4 = 0$). As expected, our model predicts that the amount of phosphorylated *EnvZ* increases with more vigorous autokinase activity (β_2) and decreases with stronger phosphotransfer activity of the histidine kinase (β_3).

Finally, while our analysis demonstrates the existence of a single robust equilibrium of the system (Theorem 1), it is instructive to consider the possibility of using such a building block as part of a closed-loop system with positive retroactivity, which could lead to oscillatory or bistable behaviors (Igoshin et al., 2008; Zorzan et al., 2021; Tiwari et al., 2010).

5.1 Phosphotransfer and reverse phosphotransfer reactions

Bifunctional sensor histidine kinase exerts both positive and negative control through SHK phosphotransfer and phosphatase activity, respectively. While the biochemical reactions underlying SHK kinase activity are reasonably well understood, the mechanisms of phosphatase activity represent a long-standing question, the investigation of which has led to the formulation of multiple hypotheses (see Huynh and Stewart, 2011 for an overview). An early hypothesis, first proposed by Dutta and Inouye (1996), identified reverse transfer of the phosphoryl group from phosphorylated RR to SHK as a potential RR dephosphorylation mechanism. Such a hypothesis was prompted by experimental results conducted on EnvZ/OmpR system in E. coli (Dutta and Inouye, 1996; Zhu et al., 2000), showing that reverse transfer of the phosphoryl group from OmpR-P to EnvZ was detected in the early period of the phosphatase reaction with domain A of EnvZ—specifically with the EnvZ kinase phosphatase mutant (EnvZ.N347D), and, under certain conditions, with wild-type *EnvZ*.

Even if later experiments invalidated the reverse phosphotransfer model (Hsing and Silhavy, 1997), it is universally recognized that reverse phosphotransfer can occur under certain conditions. As pointed out by Gao and Stock (2009), multiple mechanisms may have evolved for phosphatase activities, and individual histidine kinases may utilize different regulatory strategies. We now aim to theoretically investigate a scenario in which both direct and reverse phosphotransfer reactions occur, and a distinct phosphatase activity of the sensor histidine is present.

Since the kinase activity of SHK takes the form of a phosphotransfer reaction (by which a phosphoryl group is transferred from phosphorylated SHK to RR), reaction rates α_4 and β_3 are actually equal— $\alpha_4 = \beta_3$. We first assume that only SHK exhibits phosphotransfer activity ($\beta_4 = 0$), and we rename α_3 as α_3^p , where superscript p stands for "phosphatase activity" (of the SHK).

⁵ As reported, for instance, in (Hsing and Silhavy, 1997), in vivo OmpR is nearly 100-fold more abundant than EnvZ.

It follows from Theorem 2 that when total *RR* concentration is sufficiently high, steady-state absolute concentrations are given by $\mathbb{F}_{eq}^* = \frac{\frac{1}{4}\alpha_2 + \beta_2}{\sigma^p}$ and $s_{eq}^* = \lambda \frac{\beta_2}{\beta_c}$.

 $\mathbb{E}_{eq}^* = \frac{\frac{1}{2}\alpha_2 + \beta_2}{\alpha_3^p}$ and $s_{eq}^* = \lambda \frac{\beta_2}{\beta_3}$.

When reverse phosphotransfer from phosphorylated *RR* to *SHK* occurs, the reaction rate β_4 is non-zero and $\alpha_3 = \alpha_3^p + \alpha_3^{rt}$, with $\alpha_3^{rt} = \beta_4$ (where superscript rt stands for "reverse phosphotransfer"). Then, recalling that $\alpha_4 = \beta_3$, Theorem 2 yields

$$\begin{split} r_{eq}^{\star} &= \frac{\frac{1}{\lambda}\alpha_2 + \beta_2}{\alpha_3^p} \quad \text{and} \quad s_{eq}^{\star} &= \lambda \frac{\beta_2}{\beta_3} + \frac{\alpha_2\beta_4 + \lambda \alpha_3^{rt}\beta_2}{\alpha_3^p\beta_3} \\ &= \lambda \frac{\beta_2}{\beta_3} + \frac{\alpha_3^{rt} \left(\alpha_2 + \lambda \beta_2\right)}{\alpha_3^p\beta_3} \end{split}$$

This indicates that, even if reverse phosphotransfer occurs, the absolute concentration of phosphorylated RR remains unchanged. While this may seem contradictory at first, it is easily explained by noting that reverse phosphotransfer from phosphorylated RR to SHK is exactly compensated by the increased direct phosphotransfer from phosphorylated SHK to RR. On the contrary, when the reverse phosphotransfer reaction occurs, our analysis shows that the absolute concentration of SHK increases and that such an increase is larger for higher values of the reverse phosphotransfer rate (bigger α_3^{rt}) and/or for larger amounts of total SHK concentration (bigger λ).

This study's main findings are summarized here in comparison with the literature.

6 Conclusion

We here developed a generalized mathematical model for bacterial two-component signaling systems that integrates canonical phosphorylation cycles, bifunctional enzymatic activities, transcriptional feedback, and potential auxiliary interactions. Through systems-level analysis, we elucidated how network architecture and parameter regimes shape key dynamic properties and robustness.

Our modeling framework provides a predictive foundation for interpreting experimental dynamics, as illustrated for the EnvZ/OmpR system, and for guiding the rational design of synthetic signaling circuits. We demonstrated that the bifunctionality of the sensor histidine kinase, multi-step phosphorelays, and transcriptional feedback, which are incorporated into the model, enable rich behaviors that allow TCSs to precisely tune cellular responses to diverse environmental stimuli.

Notably, we derived analytical conditions in Propositions 3, Propositions 4, Propositions 5 and Theorem 1 under which the steady-state levels of phosphorylated proteins exhibit input–output robustness, overshoot, or bistability. We also characterized in Sections 3–4 how the equilibrium phosphorylation levels depend on the absolute and relative abundances of the two components. These insights are critical for understanding natural mechanisms of bacterial adaptation and for forward-engineering synthetic gene circuits with prescribed dynamics.

By combining the mechanistic modeling framework with systems analysis techniques, such as nullcline analysis, this study provides a unified perspective on the structural design principles that underlie the remarkable versatility of two-component signal transduction. The proposed generalized model lays a theoretical foundation for further experimental investigations, such as exploring reverse phosphotransfer mechanisms, and establishes a framework for rationally harnessing two-component systems in synthetic biology applications.

Data availability statement

The original contributions presented in the study are included in the article/supplementary material; further inquiries can be directed to the corresponding author.

Author contributions

IZ: Writing – original draft, Methodology, Formal Analysis, Investigation, Conceptualization, Visualization. CC: Methodology, Writing – review and editing, Formal Analysis, Visualization. LS: Funding acquisition, Resources, Supervision, Methodology, Writing – original draft, Conceptualization. MB: Visualization, Project administration, Investigation, Supervision, Writing – review and editing.

Funding

The author(s) declare that no financial support was received for the research and/or publication of this article.

Conflict of interest

The authors declare that the research was conducted in the absence of any commercial or financial relationships that could be construed as a potential conflict of interest.

Generative Al statement

The author(s) declare that no Generative AI was used in the creation of this manuscript.

Any alternative text (alt text) provided alongside figures in this article has been generated by Frontiers with the support of artificial intelligence and reasonable efforts have been made to ensure accuracy, including review by the authors wherever possible. If you identify any issues, please contact us.

Publisher's note

All claims expressed in this article are solely those of the authors and do not necessarily represent those of their affiliated organizations, or those of the publisher, the editors and the reviewers. Any product that may be evaluated in this article, or claim that may be made by its manufacturer, is not guaranteed or endorsed by the publisher.

References

Alvarez, A. F., and Georgellis, D. (2023). Environmental adaptation and diversification of bacterial two-component systems. *Curr. Opin. Microbiol.* 76, 102399. doi:10.1016/j.mib.2023.102399

Batchelor, E., and Goulian, M. (2003). "Robustness and the cycle of phosphorylation and dephosphorylation in a two-component regulatory system,", 100. Proceedings of the National Academy of Sciences, (Washington, D.C., USA: National Academy of Sciences), 691–696. doi:10.1073/pnas.0234782100

Blanchini, F., and Miani, S. (2015). Set-theoretic methods in control systems and control: Foundations and applications. Basel, Switzerland: Birkhäuser Basel.

Dutta, R., and Inouye, M. (1996). Reverse phosphotransfer from OmpR to EnvZ in a kinase-/phosphatase+ mutant of EnvZ (EnvZ.N347D), a bifunctional signal transducer of *Escherichia coli. J. Biol. Chem.* 271, 1424–1429. doi:10.1074/jbc.271. 31474

Gao, R., and Stock, A. (2009). Biological insights from structures of two-component proteins. *Annu. Rev. Microbiol.* 63, 133–154. doi:10.1146/annurev.micro.091208. 073214

Goulian, M. (2010). Two-component signaling circuit structure and properties. *Curr. Opin. Microbiol.* 13, 184–189. doi:10.1016/j.mib.2010.01.009

Groisman, E. (2016). Feedback control of two-component regulatory systems. *Annu. Rev. Microbiol.* 70, 103–124. doi:10.1146/annurev-micro-102215-095331

Hsing, W., and Silhavy, T. (1997). Function of conserved histidine-243 in phosphatase activity of EnvZ, the sensor for porin osmoregulation in *Escherichia coli. J. Bacteriol.* 179, 3729–3735. doi:10.1128/jb.179.11.3729-3735.1997

Huynh, T., and Stewart, V. (2011). Negative control in two-component signal transduction by transmitter phosphatase activity. *Mol. Microbiol.* 82, 275–286. doi:10.1111/j.1365-2958.2011.07829.x

Igoshin, O., Alves, R., and Savageau, M. (2008). Hysteretic and graded responses in bacterial two-component signal transduction. $Mol.\ Microbiol.\ 68,\ 1196-1215.\ doi:10.\ 1111/j.1365-2958.2008.06221.x$

Kirby, J. R. (2009). Chemotaxis-like regulatory systems: unique roles in diverse bacteria. *Annu. Rev. Microbiol.* 63, 45–59. doi:10.1146/annurev.micro.091208.073221

Mitrophanov, A., Hadley, T., and Groisman, E. (2010). Positive autoregulation shapes response timing and intensity in two-component signal transduction systems. *J. Mol. Biol.* 401, 671–680. doi:10.1016/j.jmb.2010.06.051

Mukherji, S., and van Oudenaarden, A. (2009). Synthetic biology: understanding biological design from synthetic circuits. *Nat. Rev. Genet.* 10, 859–871. doi:10.1038/nrs2697

Müller, M. M., Arndt, K. M., and Hoffmann, S. A. (2025). Genetic circuits in synthetic biology: broadening the toolbox of regulatory devices. *Front. Synthetic Biol.* 3, 1548572. doi:10.3389/fsybi.2025.1548572

Pasotti, L., Bellato, M., Casanova, M., Zucca, S., Cusella De Angelis, M. G., and Magni, P. (2017). Re-using biological devices: a model-aided analysis of interconnected transcriptional cascades designed from the bottom-up. *J. Biol. Eng.* 11, 50. doi:10. 186/s13036-017-0090-3

Ramos, A. L., Aquino, M., García, G., Gaspar, M., de la Cruz, C., Saavedra-Flores, A., et al. (2022). Rpus/r is a novel two-component signal transduction system that regulates the expression of the pyruvate symporter mctp in Sinorhizobium fredii ngr234. *Front. Microbiol.* 13, 871077. doi:10.3389/fmicb.2022.871077

Rao, S., and Igoshin, O. (2021). Overlaid positive and negative feedback loops shape dynamical properties of phopq two-component system. *PLoS Comput. Biol.* 17, e1008130. doi:10.1371/journal.pcbi.1008130

Ray, J., and Igoshin, O. (2010). Adaptable functionality of transcriptional feedback in bacterial two-component systems. *PLOS Comput. Biol.* 6, e1000676–10. doi:10.1371/journal.pcbi.1000676

Sastry, S. (1999). Nonlinear systems. Analysis, stability, and control. Interdiscip. Appl. Math. 10. doi:10.1007/978-1-4757-3108-8

Shinar, G., Milo, R., Martínez, M., and Alon, U. (2007). "Input-output robustness in simple bacterial signaling systems,", 104. Proceedings of the National Academy of Sciences, (Washington, D.C., USA: National Academy of Sciences), 19931–19935. doi:10.1073/pnas.0706792104

Stock, A., Robinson, V., and Goudreau, P. (2000). Two-component signal transduction. *Annu. Rev. Biochem.* 69, 183–215. doi:10.1146/annurev.biochem.69.1.183

Tierney, A. R., and Rather, P. N. (2019). Roles of two-component regulatory systems in antibiotic resistance. *Future Microbiol.* 14, 533–552. doi:10.2217/fmb-2019-0002

Tiwari, A., Balazsi, G., Gennaro, M., and Igoshin, O. (2010). The interplay of multiple feedback loops with post-translational kinetics results in bistability of mycobacterial stress response. *Phys. Biol.* 7, 036005. doi:10.1088/1478-3975/7/3/036005

Tiwari, S., Jamal, S. B., Hassan, S. S., Carvalho, PVSD, Almeida, S., Barh, D., et al. (2017). Two-component signal transduction systems of pathogenic bacteria as targets for antimicrobial therapy: an overview. *Front. Microbiol.* 8, 1878. doi:10.3389/fmicb. 2017.01878

Zhu, Y., Qin, L., Yoshida, T., and Inouye, M. (2000). Phosphatase activity of histidine kinase EnvZ without kinase catalytic domain. *Proc. Natl. Acad. Sci.* 97, 7808–7813. doi:10.1073/pnas.97.14.7808

Zorzan, I., Del Favero, S., Giaretta, A., Manganelli, R., Di Camillo, B., and Schenato, L. (2021). Mathematical modelling of sige regulatory network reveals new insights into bistability of mycobacterial stress response. *BMC Bioinforma*. 22, 558. doi:10.1186/s12859-021-04372-5

Zschiedrich, C., Keidel, V., and Szurmant, H. (2016). Molecular mechanisms of two-component signal transduction. *J. Mol. Biol.* 428, 3752–3775. doi:10.1016/j.jmb.2016. 08.003